

Structure, mechanical and thermodynamic stability of vacancy clusters in Cu

Qing Peng, Xu Zhang and Gang Lu

Department of Physics and Astronomy, California State University Northridge, Northridge, CA, USA

(Dated: April 8, 2018)

The atomic structure, mechanical and thermodynamic stability of vacancy clusters in Cu are studied by atomistic simulations. The most stable atomic configuration of small vacancy clusters is determined. The mechanical stability of the vacancy clusters is examined by applying uniaxial and volumetric tensile strain to the system. The yield stress and yield strain of the system are significantly reduced comparing to the perfect lattice. The dependence of vacancy formation and binding energy as a function of strain is explored and can be understood from the liquid-drop model. We find that the formation energy of the vacancy clusters decreases monotonically as a function of the uniaxial strain, while the formation energy increases first then decreases under the volumetric tensile strain. The thermodynamic stability of the vacancy clusters is analyzed by calculating the Gibbs free binding energy and the total probability of dissociation of the vacancy clusters at 300 K and 900 K under uniaxial and volumetric strains. We find that although most of the vacancy clusters appear to be thermodynamically stable, some of the immediate sized clusters have high probability of dissociation into smaller clusters.

PACS numbers: 61.72.Bb,61.72.jd,61.72.J-,61.72.-y

I. INTRODUCTION

Vacancies are predominant point defects in metals and they could have profound influence on materials properties, ranging from mechanical strength^{1,2,3}, deformation behavior^{4,5}, kinetic transport and diffusion^{6,7}, to electrical conductivity and heat capacity^{8,9}, to name a few. Thus the study of vacancy effects on properties of technologically important materials, such as Cu, is of great interest. For all these properties, stress plays crucial roles. For example, it is generally believed that hydrostatic tensile stress is the driving force for the stress-void nucleation¹⁰ and stress gradients are responsible for the void growth¹¹. The present work touches upon the stress induced voiding, which is one of the most important factors that cause failures of ultra-large integrated circuits with Cu-based interconnects¹². In this case, the stress is built up as a result of the mismatch in thermal expansion coefficients between the metal lines and the surrounding dielectrics¹³. There are other interesting problems related to the void growth and coalescence under various loading conditions^{14,15,16,17,18,19}. For example, experimentally TEM observations have been performed for neutron-irradiated Cu at 300°C which verify the transition from stacking fault tetrahedra (SFT) to voids, depending on the size of the vacancy cluster. These observations are consistent to the embedded-atom-method (EAM) simulations^{20,21}. A direct transition from a 20-vacancy cluster to an SFT was also found by using parallel replica EAM molecular dynamics simulations¹⁶. We have recently studied void formation by using multiscale method and discovered a connection between vacancy-induced bonding cage and the tendency of void formation in fcc metals²².

In this paper, we will use atomistic simulations based on EAM potential to (1) determine the structure of the most stable n -vacancy clusters where $n \leq 21$; (2) ex-

amine the mechanical stability of Cu containing vacancy clusters; (3) study the dependence of vacancy-cluster formation energy and binding energy as a function of uniaxial and volumetric tensile stress; (4) examine the thermal stability of the vacancy-clusters at different temperatures. The computational method is given in Sec II. The convergence of vacancy formation energy is studied in Sec III(A); the structure of vacancy clusters is determined in Sec III(B) and the mechanical stability of the vacancy clusters is examined in Sec. III(C) for both uniaxial and volumetric tensile strains. Finally the thermal stability of the vacancy clusters is considered in III(D) and the conclusion is in Sec IV.

II. COMPUTATIONAL METHOD

A cubic supercell with periodic boundary conditions along three directions is used in the simulations. The supercell is oriented in cubic directions, i.e., x in [100], y in [010] and z in [001], respectively. The atomic interaction is described by Ercolessi-Adams EAM potential²³, which has been widely used for the metallic systems, such as Cu^{4,14,15,16,17,18,20,21,24}. The atomic relaxation is carried out with molecular statics implemented in the LAMMPS codes²⁵. It is well established that the EAM potential is capable to provide reasonable atomic structure and energetics for vacancies in Cu^{14,16,17}.

The vacancy cluster formation energy, which describes the energy cost for forming a vacancy cluster with respect to the perfect lattice, is computed for various vacancy clusters, in the presence or absence of external strains. Specifically, under a strain ϵ the vacancy cluster formation energy, $E_{nv,\epsilon}^F$ of a given n -vacancy cluster in an N -atom supercell is defined as

$$E_{nv,\epsilon}^F = E_{nv,\epsilon}^{\text{tot}}(N - n) - \frac{N - n}{N} E_{0,\epsilon}^{\text{tot}}(N), \quad (1)$$

where $E_{nv,\epsilon}^{\text{tot}}(N-n)$ is the total energy of the supercell containing $(N-n)$ atoms with an n -vacancy cluster under strain ϵ and $E_{0,\epsilon}^{\text{tot}}(N)$ is the total energy of the supercell containing N atoms in a perfect lattice with a strain of ϵ . It is convenient to use the formation energy per vacancy $E_{nv,\epsilon}^{\text{f}}$ to compare among different vacancy clusters, which is defined as

$$E_{nv,\epsilon}^{\text{f}} = E_{nv,\epsilon}^{\text{F}}/n. \quad (2)$$

Another important quantity calculated is the vacancy binding energy, $E_{nv,\epsilon}^{\text{B}}$, which describes the energy gain when n monovacancies are combined into an n -vacancy cluster. The binding energy of an n -vacancy cluster under a strain ϵ is given by

$$E_{nv,\epsilon}^{\text{B}} = nE_{1v,\epsilon}^{\text{f}} - E_{nv,\epsilon}^{\text{F}}. \quad (3)$$

A positive value of $E_{nv,\epsilon}^{\text{B}}$ suggests that it is energetically favorable for the n monovacancies to form an n -vacancy cluster at zero temperature under the strain. Similarly, one can define the binding energy per vacancy, $E_{nv,\epsilon}^{\text{b}}$, to facilitate the comparison among different vacancy clusters, which is given by

$$E_{nv,\epsilon}^{\text{b}} = E_{nv,\epsilon}^{\text{B}}/n = E_{1v,\epsilon}^{\text{f}} - E_{nv,\epsilon}^{\text{f}}. \quad (4)$$

In order to determine the thermodynamic stability of a vacancy cluster, we need to calculate dynamical matrix and free energy of the defect system. Under the harmonic approximation, the dynamical matrix under strain ϵ is defined as following

$$D_{i,j}^{\alpha,\beta} = \frac{1}{m} \frac{\partial^2 E_{\epsilon}^{\text{tot}}}{\partial u_i^{\alpha} \partial u_j^{\beta}}, \quad (5)$$

where m is the mass of the atoms, u_i^{α} and u_j^{β} are the displacement of atom i and j in direction α and β , respectively from its relaxed equilibrium position. $E_{\epsilon}^{\text{tot}}$ is the total energy of the system. The vacancy formation entropy is evaluated via the equation^{26,27}

$$S_{nv,\epsilon}^{\text{F}} = -k_{\text{B}} \left(\sum_{i=1}^{3(N-n-1)} \ln \omega_i^{nv,\epsilon} - \frac{N-n-1}{N-1} \sum_{i=1}^{3(N-1)} \ln \omega_i^{0,\epsilon} \right), \quad (6)$$

where $\omega_i^{nv,\epsilon}$ and $\omega_i^{0,\epsilon}$ represents the harmonic vibrational frequency for the system with and without vacancies, respectively. Three acoustic phonon frequencies are removed from the sum owing to the translational invariance of the system. Analogous to the definition of the binding energy, the binding entropy is defined as

$$S_{nv,\epsilon}^{\text{B}} = nS_{1v,\epsilon}^{\text{F}} - S_{nv,\epsilon}^{\text{F}}, \quad (7)$$

where $S_{1v,\epsilon}^{\text{F}}$ and $S_{nv,\epsilon}^{\text{F}}$ are the formation entropy of a monovacancy and an n -vacancy cluster, respectively.

The dynamical matrix is determined by displacing the atoms $\pm 0.01\text{\AA}$ from their relaxed equilibrium positions in

all three Cartesian directions.²⁷ The dynamical matrix is then diagonalized and the eigen-frequencies are obtained to evaluate the formation entropy. The Gibbs binding free energy of an n -vacancy cluster at temperature T is determined as

$$G_{nv,\epsilon}^{\text{B}} = E_{nv,\epsilon}^{\text{B}} - TS_{nv,\epsilon}^{\text{B}}, \quad (8)$$

The positive (negative) value of $G_{nv,\epsilon}^{\text{B}}$ indicates the n -vacancy cluster is thermodynamically stable (unstable) against a simultaneous dissociation into n monovacancies.

III. RESULTS AND ANALYSIS

A. Convergence of vacancy formation energy

A convergence test is carried out to determine the sufficient system size, and results are shown in Fig. (1). For a monovacancy, we find $6a_0$ ($a_0 = 3.615 \text{ \AA}$) is enough to reach convergence for the vacancy formation energy, while for 21-vacancy cluster (the largest vacancy cluster in this study), $20a_0$ appears to be sufficient. Therefore, in all our calculations, we use $20a_0$ as the system size. With a supercell of $20a_0 \times 20a_0 \times 20a_0$ (32000 lattice sites), we found that the monovacancy formation energy is 1.2837 eV, which agrees very well with previous calculation and experiment^{28,29}.

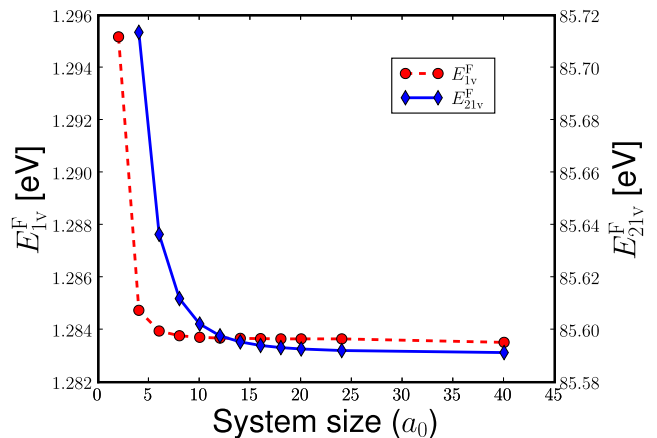


FIG. 1: (Color online) The convergence test of the vacancy formation energy with respect to the system size for a monovacancy (dashed line, scaled to the left axis) and a 21-vacancy cluster (solid line, scaled to the right axis).

B. Atomic structure of n -vacancy clusters

The vacancy clusters containing up to twenty-one vacancies are studied in this work. For each n -vacancy cluster

ter, several most stable configurations are considered, especially in planar, tetrahedral, and spherical structures. These structures are emphasized owing to their relevance to vacancy loops, stacking fault tetrahedra and spherical voids, observed in experiments¹. For each n , the structure with the maximum binding energy is regarded as the most energetically stable configuration for the n -vacancy cluster.

The most stable di-vacancy is the one that the two vacancies are the nearest neighbors. The binding energy is 0.158 eV, agreeing well with the previous calculation and experiment^{28,29}. Starting from the most stable di-vacancy, we can search for the most stable tri-vacancy by placing the third vacancy at various nearest-neighbor position. The configuration of the highest binding energy of a tri-vacancy is shown in Fig. 2(a) and $E_{3v}^B = 0.474$ eV. The three vacancies form an equilateral triangle lying on $\{111\}$ plane, and are mutually nearest-neighbors. Starting from the most stable tri-vacancy, we considered six most probable configurations for a four-vacancy cluster, and found that the equilateral tetrahedron formed by four nearest-neighbor vacancies has the highest binding energy of $E_{4v}^B = 0.94$ eV. The atomic structure of the tetra-vacancy is shown in Fig. 2(b).

In the same manner, we explored the most stable atomic configurations for all vacancy clusters with $n \leq 21$. For example, we found the most stable 5-vacancy cluster (penta-vacancy) is a squared pyramid with a binding energy of $E_{5v}^B = 1.372$ eV, shown in Fig. 2(c). The most stable 6-vacancy cluster (hexa-vacancy) is an octahedron shown in Fig. 2(d) with a binding energy of $E_{6v}^B = 2.113$ eV. Interestingly, we found that the most stable configuration of a 10-vacancy cluster is not an equilateral tetrahedron shown in Fig. 2(e), but rather a less symmetric structure shown in Fig. 2(f). For $n = 13$, the most stable structure resembles a sphere, with one vacancy at the center, and 12 nearest neighbors surrounding it. The radius of the sphere is $\sqrt{2}/2a_0$ shown in Fig. 2(g). For $n > 13$, the vacancy clusters tend to form 3-dimensional voids, appearing more like spheres than tetrahedra. For example, the structure of a 19-vacancy cluster is shown in Fig. 2(h); it has one vacancy at center, and 12 nearest neighbors and 6 second-nearest neighbors of the central vacancy filling the sphere of a radius of a_0 .

The formation energy per vacancy E_{nV}^f for all vacancy clusters is presented in Fig. 3. Overall, the formation energy decreases with respect to the cluster size, which can be understood from the liquid-drop model for metals^{30,31}. In this model, the void formation energy can be approximated as

$$E_{\text{void}}^F = 4\pi R_{\text{WS}}^2 \sigma - 2\pi R_{\text{WS}} \gamma, \quad (9)$$

where $R_{\text{WS}} = (3V/4\pi)^{1/3}$ is the Wigner-Seitz radius of the void with volume V , σ is the surface energy density, and γ is the curvature energy³⁰. The volume of an n -vacancy cluster can be approximated as $V_n \approx nv_0$, where v_0 is the volume of a monovacancy. Therefore the Eq. (9)

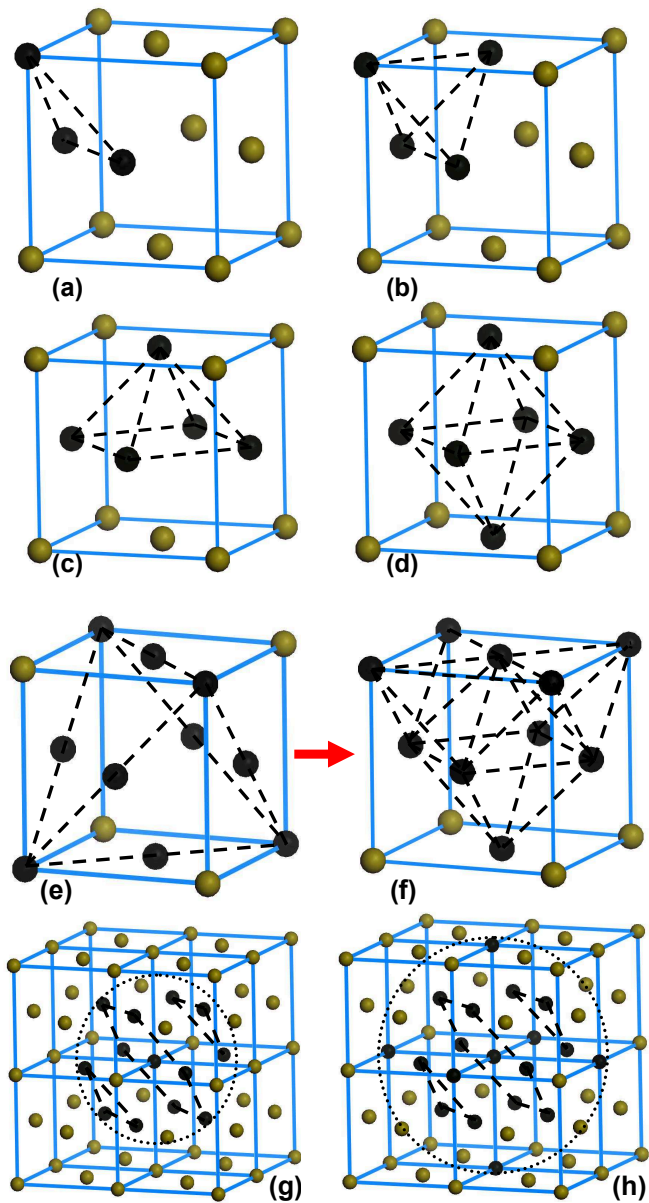


FIG. 2: The most stable atomic configurations for 3, 4, 5, 6, 10, 13, and 19-vacancy clusters. The black circle represents for the vacancy and the brown circle for the atoms. Note that the most stable configuration for the 10-vacancy cluster is not the symmetrical one shown in (e), but rather the one with less symmetry shown in (f).

can be rewritten as

$$E_{nv}^f = c_1 n^{-\frac{1}{3}} - c_2 n^{-\frac{2}{3}}, \quad (10)$$

where $c_1 = 4\pi\sigma(3v_0/4\pi)^{2/3}$, $c_2 = 2\pi\gamma(3v_0/4\pi)^{1/3}$. Taking $\sigma = 0.0932$ eV/Å², $\gamma = 0.119$ eV/Å, and $v_0 = a_0^3/4$, the Eq. (10) is plotted in Fig. (3), which matches very well the atomistic results. The value of σ and γ is taken from reference³⁰. σ is close to the EAM surface energy density of Cu: 0.08 eV/Å² for (110) surface and 0.114 eV/Å² for (111) surface. Interestingly, we find that the

formation energy curve becomes flatter as n becomes larger, and approaches an asymptotic value of 0.7 eV. This value is very close to the monovacancy formation energy on a flat (111) surface of Cu, which is 0.73 eV. The reason for this asymptotic behavior is that as the vacancy cluster becomes larger, the curvature of the void surface becomes smaller, and thus the formation energy approaches the value of a monovacancy on a flat surface.

We also present the binding energy per vacancy as a function of n in Fig. 3, shown in diamond curve and scaled to the right axis. The binding energy increases monotonically with n , and is positive for all vacancy clusters, suggesting that the monovacancies prefer to aggregate in Cu, in order to reduce the number of broken bonds. From Eq. (10) and Eq. (4), we can express E_{nv}^b as

$$E_{nv}^b = c_1(1 - n^{-\frac{1}{3}}) - c_2(1 - n^{-\frac{2}{3}}), \quad (11)$$

which is plotted as the dashed line in Fig. (3). It appears that the liquid-drop model reproduces the atomistic results surprisingly well.

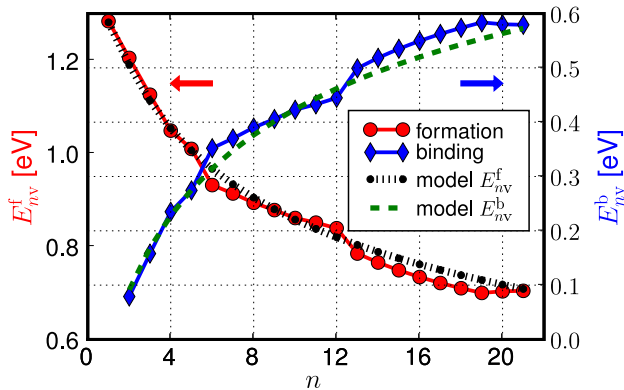


FIG. 3: The formation energy (circle, scaled to left) and binding energy (diamond, scaled to right) per vacancy of the n -vacancy clusters. The dot-dashed line and dashed line are the prediction of E_{nv}^f and E_{nv}^b from the liquid-drop model respectively.

C. Mechanical stability

In this section, we examine the mechanical stability of the vacancy clusters by applying external uniaxial tensile strain and volumetric tensile strain to the system. The strain-free structures of the vacancy clusters are taken from the results obtained in Sec. B.

1. Uniaxial tensile strain

The uniaxial tensile strain is applied along the y axis, and the x and z axes are free to change by conserving

the volume. The strain is applied quasi-statically, with each loading that is 1.001 times that of the previous step. We examine the mechanical response of the vacancy clusters by showing the strain energy and tensile stress σ_{yy} as a function of applied strain ϵ_{yy} . Because the results of all vacancy clusters follow the same pattern, we select the 13-vacancy cluster as a representative to illustrate the salient features of the results. As shown in Fig. 4, we find that both strain energy and the tensile stress increase monotonically with strain initially, followed by a sudden drop at the yield point. The system behaves in a linear elastic fashion, i.e., the energy increases quadratically and the stress increases linearly. There are two importance results: (1) the perfect and the defect lattice have almost identical elastic behavior - the two curves coincide with each other for both energy and stress. (2) The presence of the vacancy defect significantly reduces the yield strength of the material. The yield stress and strain are 7.32 GPa and 0.117 for the perfect lattice, and 4.98 GPa and 0.085 for the defect system, respectively. At the yield point (the drop in the curves), dislocations are nucleated and propagate through the system, evidenced by the Central Symmetry Parameter (CSP)^{4,32} plot in

Fig. 5. CSP is defined as $CSP = \sum_{i=1}^6 |R_i + R_{i+6}|^2 / 24D^2$, where R_i and R_{i+6} are the vectors or bonds corresponding to the six pairs of opposite nearest neighbors in the deformed fcc lattice³², and D is the nearest neighbor distance in the perfect fcc lattice. For each atom, there is a CSP value associated with it. Dislocation core and stacking fault correspond to the CSP values ranging between 0.003 and 0.1. Just before the yielding, there is no dislocation in the system (Fig. 5a) while just after the yielding, dislocations appear (Fig. 5b).

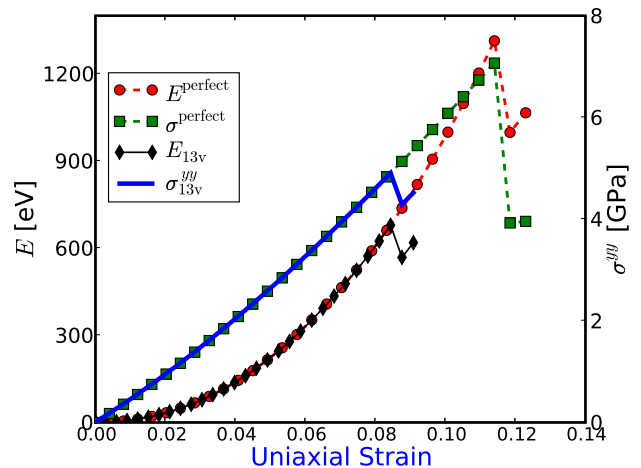


FIG. 4: The strain energy (scale to the left axis) and stress (scale to the right axis) vs. uniaxial tensile strain for a 13-vacancy cluster (diamond and solid line) and perfect lattice(circle and square) respectively.

In Fig. 6, we present the yield strain (left axis) and

yield stress (right axis) as a function of n . Overall, the yield strain traces approximately the yield stress, and for large vacancy clusters, the yield stress/strain is significantly reduced comparing to the perfect lattice. However, the vacancy effect on the mechanical strength is more complex than the simple monotonic behavior. More atomistic studies are required to unravel the complicated vacancy-dislocation interactions.

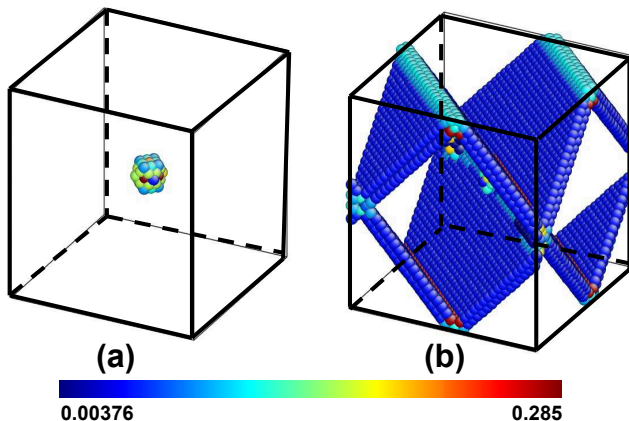


FIG. 5: CSP plot for the system immediately before (a) and after (b) the yield point. The color bar represents the magnitude of CSP values in the system.

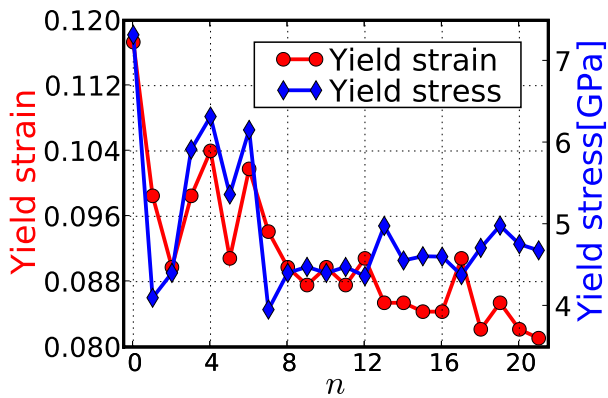


FIG. 6: The yield strain (circle, scaled to the left) and yield stress (diamond, scaled to the right) of n -vacancy clusters under uniaxial strain.

We have calculated the formation energy $E_{nv,\epsilon}^f$ of the vacancy clusters under uniaxial strain up to 0.062 beyond which some of the defect systems start yielding. The results are summarized in Fig. (7) for representative vacancy clusters - the results of all vacancy clusters have the same general features. It is found that the formation energy decreases monotonically as a function of strain for all clusters. This is because vacancy formation energy results from the energy cost of bond breaking around the vacancies. By applying tensile stress, the

bonds are weakened owing to the stretching, therefore it would cost less energy to break them comparing to the strain-free case. The present result is consistent with that in Al obtained by orbital-free density functional theory calculations³³. It appears that some of the energy curves tend to converge (or cross) at larger strains, for example, $n = 5, 6, 10$. The apparent convergence suggests that a large stress can change the relative stability of vacancy clusters of different sizes, which may trigger structural changes among them.

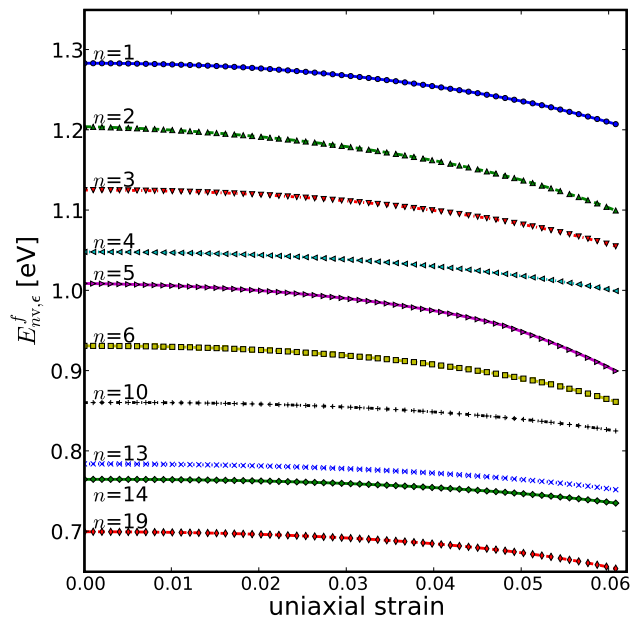


FIG. 7: The formation energy per vacancy $E_{nv,\epsilon}^f$ under uniaxial strain ϵ for several representative vacancy clusters.

The binding energy per vacancy $E_{nv,\epsilon}^b$ is shown in Fig. (8). The binding energy remains positive for all strains less than 0.062. For most of the vacancy clusters, the binding energy decreases as a function of strain because the attractive vacancies are pulled apart by the stress. It appears that large strains could lead to break-up or re-arrangement of the vacancy clusters.

2. Isotropic volumetric tensile strain

Next we study the behavior of the vacancy clusters under isotropic volumetric tensile deformations. In this case of triaxial loading, the volume of the system is no longer conserved, but with an equal strain applied along x, y, z directions simultaneously. At each deformation step, the size of the simulation box is 1.0005 times that of the previous step.

The strain energy and stress as a function of strain are shown in Fig. 9, with $n = 13$ as a representative because all vacancy clusters behave in the same way. The energy increases with the strain before the drop at a volume

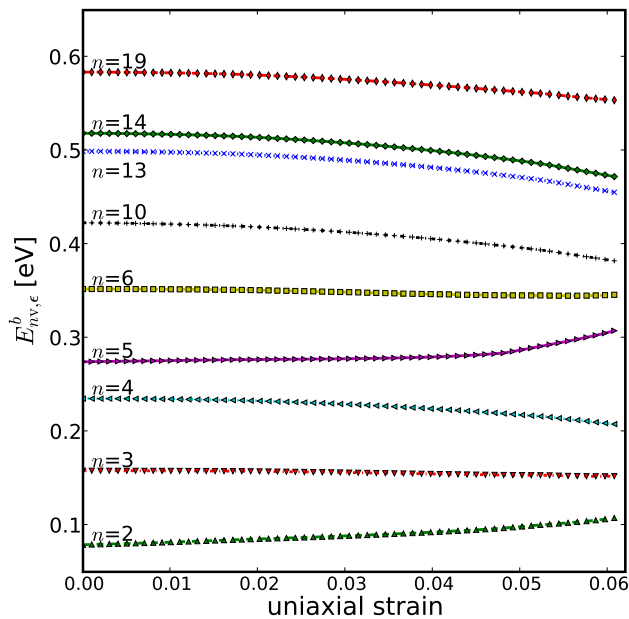


FIG. 8: The binding energy per vacancy $E_{nv,\epsilon}^b$ under uniaxial strain ϵ for several representative vacancy clusters

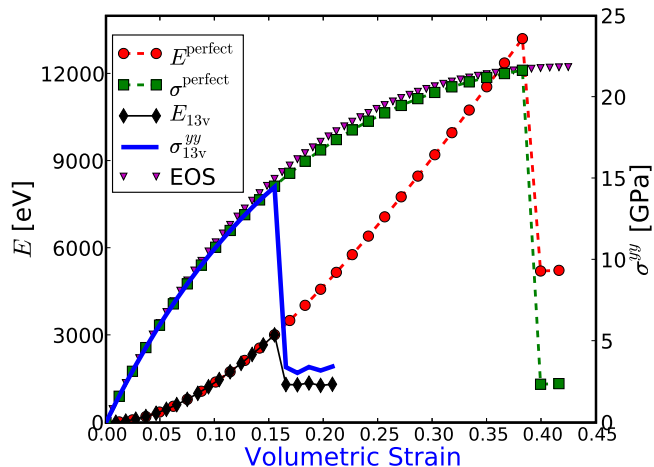


FIG. 9: The strain energy (scale to the left axis) and stress (scale to the right axis) vs. isotropic volumetric strain for a 13-vacancy cluster (diamond and solid line) and perfect lattice (circle and square) respectively. The triangle curve represents the EOS from Eq. (13).

strain of $\epsilon = 0.13$. The drop of the energy is an indication of the onset of plasticity of the system. The stress drops at the same strain as the energy. For the isotropic volumetric tensile strain, $\sigma^{yy} = \sigma^{xx} = \sigma^{zz} = -P$, and P is the pressure. The non-linear behavior of the stress-strain relation in Fig. 9 can be understood from the equation of state (EOS) of solids³⁴:

$$P(V) = \frac{3K_0(1-x)}{x^2} \exp[\xi(1-x)], \quad (12)$$

where V_0 and K_0 are the volume and the bulk modulus of the solid at equilibrium; $x \equiv (V/V_0)^{1/3}$, $\xi \equiv \frac{3}{2}(K'_0 - 1)$, and $K'_0 \equiv \frac{\partial K_0}{\partial P}|_{P=0}$. For the volumetric loading, $V = V_0(1 + \epsilon)$ and $x - 1 \approx \frac{1}{3}\epsilon$, thus we can rewrite Eq. (12) as

$$\sigma(\epsilon) = \frac{K_0\epsilon}{(1 + \epsilon/3)^2} \exp\left[-\frac{\xi\epsilon}{3}\right]. \quad (13)$$

Eq. (13) is plotted as the triangle curve in Fig. (9) and it agrees very well with the EAM data by taking the experimental value of $K_0 = 140$ GPa and $\xi = 5.2$.

The yield strain and yield stress for all vacancy clusters under the volumetric deformation are plotted in Fig. (10). The energy/stress curves of the defect systems trace closely to that of the perfect lattice, indicating the vacancy clusters do not change the behavior of the material before yielding. Overall, both the yield stress and strain decrease as a function of n , suggesting that vacancy clusters can drastically reduce the yield strength of the material. It should be noted that the quantitative values of the yield stress/strain obtained here do not correspond to the realistic situation due to the high vacancy concentrations in the simulations; however, the qualitative features remain to be valid.

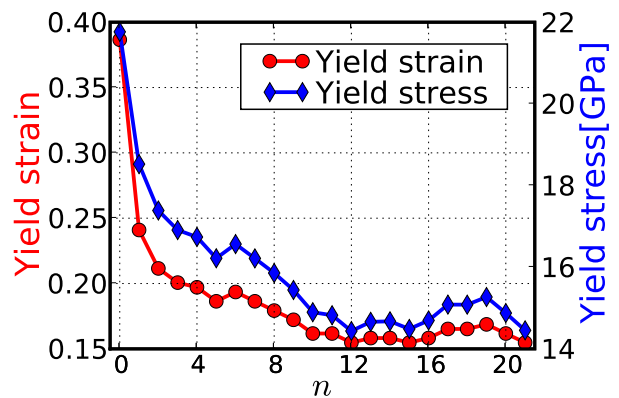


FIG. 10: The yield strain (circle, scaled to the left) and stress (cross, scaled to the right) of n -vacancy clusters under the volumetric tensile strain.

The formation energy per vacancy under the volumetric tensile strain is shown in Fig. (11). Overall, we find that the formation energy first increases with the strain to a maximum and then decreases; this is different from the uniaxial case. The difference is due to the different loading conditions: in the uniaxial case, the volume of the system is fixed, therefore to a good approximation, the surface area of the void is also fixed. On the other hand, the surface area of the void increases as the volume increases in the triaxial case, therefore the inner surface energy increases as a function of the tensile strain. The increasing surface energy dominates the decreasing bonding energy contribution at small strains, hence the formation energy reaches a maximum at an immediate

strain. For small vacancy clusters, such as $n = 1$ and $n = 2$, the surface energy contribution is negligible owing to the small size of the vacancy clusters, thus their formation energy increases monotonically.

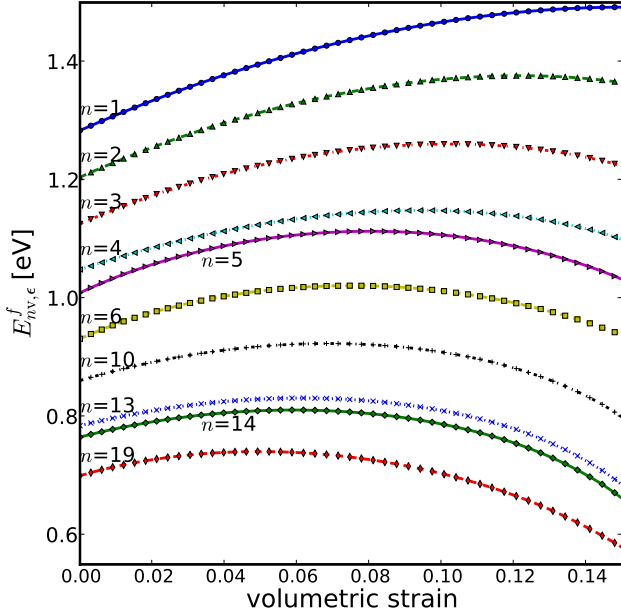


FIG. 11: The formation energy per vacancy $E_{nv,\epsilon}^f$ under the volumetric strain ϵ for several representative vacancy clusters.

For the volumetric strain, the binding energy per vacancy increases monotonically with the strain, and it increases faster when n is larger. Such a behavior can be understood again from the liquid-drop model. Under the volumetric strain ϵ , the volume of a monovacancy is $v_0(1 + \epsilon_{11})^3$ where the linear strain $\epsilon_{11} \approx \epsilon/3$. Thus the two coefficients in Eq. (11) become $c_1(1 + \epsilon_{11})^2$ and $c_2(1 + \epsilon_{11})$ respectively. $E_{nv,\epsilon}^b$ can then be expressed as a quadratic function of ϵ_{11} or ϵ :

$$\begin{aligned} E_{nv,\epsilon}^b &= c_1(1 - n^{-\frac{1}{3}})(1 + \epsilon_{11})^2 - c_2(1 - n^{-\frac{2}{3}})(1 + \epsilon_{11}) \\ &= c_1(1 - n^{-\frac{1}{3}})\epsilon_{11}^2 \\ &\quad + [2c_1(1 - n^{-\frac{1}{3}}) - c_2(1 - n^{-\frac{2}{3}})]\epsilon_{11} \\ &\quad + c_1(1 - n^{-\frac{1}{3}}) - c_2(1 - n^{-\frac{2}{3}}). \end{aligned} \quad (14)$$

Since $c_1(1 - n^{-\frac{1}{3}}) > 0$ and $[2c_1(1 - n^{-\frac{1}{3}}) - c_2(1 - n^{-\frac{2}{3}})] > 0$, $E_{nv,\epsilon}^b$ would increase monotonically with the volumetric strain ϵ . The larger the n value, the larger the coefficient of the quadratic term $c_1(1 - n^{-\frac{1}{3}})$, hence $E_{nv,\epsilon}^b$ increases faster with respect to the strain.

D. Thermodynamic Stability

Finally, we address the thermodynamic stability of the vacancy clusters. At finite temperatures T , a vacancy

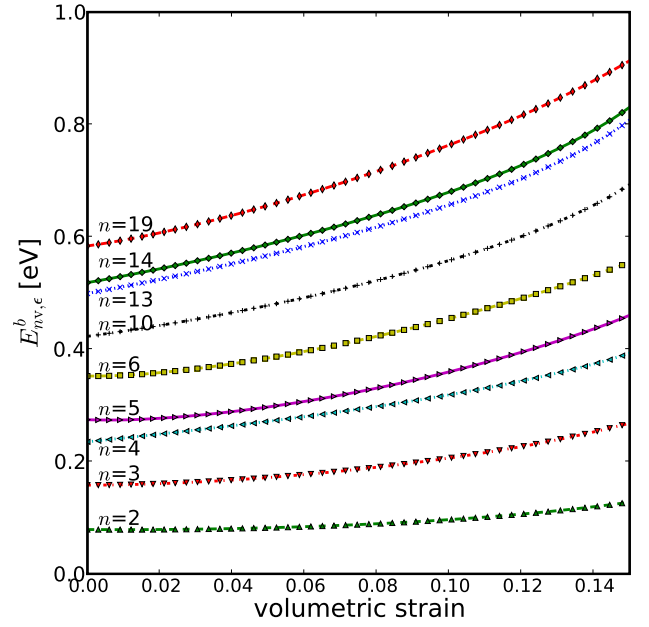


FIG. 12: The binding energy per vacancy (eV) $E_{nv,\epsilon}^b$ under volumetric strain ϵ for several representative vacancy clusters.

cluster could dissociate into smaller clusters, or eventually into monovacancies. In the following, we use the concept of total probability of dissociation $P_{\text{tot}}(n)$ ²² to analyze the thermal stability of the vacancy clusters. $P_{\text{tot}}(n)$ can be expressed as $P_{\text{tot}} = \sum_i P_i(n)$ where $P_i(n)$ represents the probability of a particular (the i th) way of dissociation. For example, an n -vacancy cluster may dissociate into n monovacancies simultaneously, whose probability, $P_1(n)$ is given by

$$\begin{aligned} P_1(n) &= \frac{(c_{1v})^n}{c_{nv}} = \frac{n}{g_{nv}} e^{-(nG_{1v,\epsilon}^F - G_{nv,\epsilon}^F)/k_B T} \\ &= \frac{n}{g_{nv}} e^{-G_{nv,\epsilon}^B/k_B T}; \end{aligned} \quad (15)$$

or an n -vacancy cluster could break into a monovacancy plus an $(n - 1)$ -vacancy cluster, whose probability $P_2(n)$ is expressed as

$$P_2(n) = \frac{c_{1v}c_{(n-1)v}}{c_{nv}} = \frac{ng_{(n-1)v}}{(n-1)g_{nv}} e^{-(G_{nv,\epsilon}^B - G_{(n-1)v,\epsilon}^B)/k_B T} \quad (16)$$

where g_{nv} is the coordination number of the n -vacancy cluster³⁵, etc. The concentration of the n -vacancy cluster is denoted by c_{nv} and k_B is the Boltzmann constant. The definition of $P_i(n)$ can be used in both thermal equilibrium condition and a constant supersaturation condition²². Here we have to consider all possible dissociation paths in calculating a given $P_{\text{tot}}(n)$. The variation of $G_{nv,\epsilon}^B$ with respect to n determines the dissociation probability²²; while an n -vacancy cluster is thermally stable under a positive and rapidly increasing $G_{nv,\epsilon}^B$ function, a negative and slowly increasing $G_{nv,\epsilon}^B$ would re-

sult in a high dissociation probability of the n -vacancy cluster.

With Eqs.(5)-(7), we can evaluate the binding entropy $S_{nv,\epsilon}^B$, and then the Gibbs binding free energy of an n -vacancy cluster $G_{nv,\epsilon}^B$ at a given temperature T . In Fig. (13), we present $G_{nv,\epsilon}^B$ at $T = 300\text{K}$ and $T = 900\text{K}$ under the uniaxial and volumetric tensile strains. From the Gibbs binding free energy, one can estimate the total dissociation probability $P_{\text{tot}}(n)$ of an n -vacancy cluster. The calculation reveals that the total dissociation probabilities of all n -vacancy clusters, except $n = 14$, are much less than 0.5 under both strain-free and volumetric tensile strain conditions, which means they are thermodynamically stable. On the other hand, under the volumetric strain, the 14-vacancy cluster has more than 50% probability to dissociate into a 13-vacancy cluster and a mono-vacancy because $G_{14v,\epsilon}^B$ is smaller than $G_{13v,\epsilon}^B$. Under a uniaxial tensile strain, 10- and 11-vacancy clusters are not stable at $T = 900\text{K}$; the 10- or 11-vacancy cluster has a high probability to dissociate into two 5-vacancy clusters or one 5- and one 6-vacancy clusters, respectively.

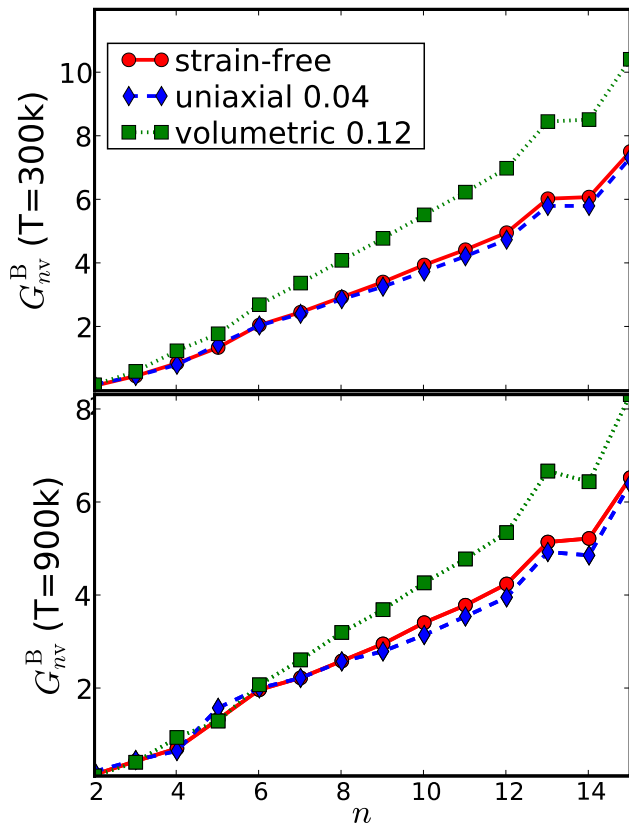


FIG. 13: The Gibbs binding free energy of n -vacancy clusters at different temperatures for strain-free (circle), uniaxial tensile strain (diamond) and volumetric tensile strain (square).

IV. CONCLUSION

We have examined structure, mechanical and thermodynamic stability of n -vacancy clusters where n goes from 2 to 21. We determine the most stable atomic structure of the vacancy clusters based on simple intuitive considerations and energetic calculations. More extensive (such as global search) and accurate (such as quantum mechanical) calculations are required to settle the issue with more confidence. The present work should only be considered as a preliminary effort. We find that the formation energy per vacancy decreases while the binding energy increases as a function of cluster size n . We probe the mechanical stability of the vacancy clusters by applying uniaxial and volumetric tensile strains. It is observed that yield stress and yield strain of the material are significantly reduced by the vacancy clusters. However, the presence of the vacancy cluster does not change the elastic behavior of the material before yielding. We find that formation energy per vacancy decreases as a function of uniaxial strain for all clusters, while the binding energy shows a more complicated behavior. For volumetric deformations, the formation energy per vacancy increases first then decreases as a function of strain. The increase of the formation energy at smaller strains is due to the increased surface energy associated with the void. We determine the thermodynamic stability of the clusters by calculating the Gibbs free binding energy and resultant probability of dissociation. We find that most of the vacancy clusters under study are thermodynamically stable except the 14-vacancy cluster, which has a high probability of dissociating into a 13-vacancy cluster and a mono-vacancy. In addition, at 900K the 10- and 11-vacancy clusters will dissociate into two 5-vacancy clusters or a 5- and a 6-vacancy clusters, respectively under a uniaxial strain.

Acknowledgments

The work at California State University Northridge was supported by NSF PREM grant DMR-0611562 and the ACS Petroleum Research Funds PRF43993-AC10.

¹ S.J. Zinkle, L.E. Seitzman and W.G. Wolfer, *Philos. Mag. A* **55**, 111 (1987)

² G. Lu and E. Kaxiras, *Phys. Rev. Lett.* **94**, 155501 (2005)

³ S. B. Fisher, R. J. White and K. M. Miller, *Philos. Mag. A* **40**, 239 (1979).

⁴ J. Marian, J. Knap and M. Ortiz, *Phys. Rev. Lett.* **93**,

- 165503 (2004).
- ⁵ G. Lu and E. Kaxiras, Phys. Rev. Lett. **89**, 105501 (2002)
 - ⁶ A. Seeger and H. Mehrer, in *Vacancies and Interstitials in Metals*, edited by A. Seeger, H. Schumacher, W. Schilling, and J. Diel (North-Holland, Amsterdam, 1970), p. 1.
 - ⁷ G. Neumann, Defect Diffus. Forum **43**, 66 (1989).
 - ⁸ C. Kittel, *Introduction to Solid State Physics*, 7th ed. (Wiley, New York, 1996).
 - ⁹ Y. Kraftmakher, Phys. Rep. **299**, 79 (1998).
 - ¹⁰ B.Z. Li, T.D. Sullivan, T.C. Lee and D. Badami, Microelectron Reliab. **46**, 1673 (2006)
 - ¹¹ R.C.J. Wang, C.C. Lee, L.D. Chen, K. Wu and K.S. Chang-Liao, Microelectron Reliab. **44**, 365 (2004)
 - ¹² Z.Y. Wu, Y.T. Yang, C.C. Chai, Y.J. Li, J.Y. Wang, J. Liu and B. Liu, J. Microrel. **48**, 578 (2008)
 - ¹³ T. Matsuea, T. Hanabusab, Y. Ikeuchia, K. Kusakab and O. Sakatac, Vacuum **80**, 836 (2006)
 - ¹⁴ K. Kolluri, M. R. Gungor and D. Maroudas, J. Appl. Phys. **103**, 123517 (2008)
 - ¹⁵ T.C. Tszeng, J. Appl. Phys. **103**, 053509 (2008)
 - ¹⁶ B.P. Uberuaga, R.G. Hoagland, A.F. Voter, and S. M. Valone, Phys. Rev. Lett. **99**, 135501 (2007)
 - ¹⁷ R. E. Rudd and J.F. Belak, Comp. Mater. Sci. **24** 148 (2002)
 - ¹⁸ D.C. Ahn, P. Sofronis and R. Minich, J. Mech. Phys. Solids **54**, 735 (2006)
 - ¹⁹ I. Mukouda and Y. Shimomura, J. Nucl. Mater. **271-272**, 230, (1999).
 - ²⁰ Y. Shimomura and R. Nishiguchi, Rad. Eff. Defects Solids **141**, 311 (1997)
 - ²¹ Y. Shimomura, M.W. Guinanb and T. Diaz de la Rubia, J. Nucl. Mater. **205**, 374 (1993)
 - ²² X. Zhang and G. Lu, Phys. Rev. B **77**, 174102 (2008)
 - ²³ F. Ercolessi and J.B. Adams, Europhys. Lett. **26**, 583 (1994)
 - ²⁴ Y. Shimomura, M. Kiritani and I. Mukouda, Philos. Mag. A **350**, 238 (2003)
 - ²⁵ S. J. Plimpton, J. Comp. Phys., **117**, 1 (1995)
 - ²⁶ Y. Mishin, M.R. Sorensen, and A.F. Voter, Philos. Mag. A **81**, 2591 (2001).
 - ²⁷ K.M. Carling, G. Wahnström, T.R. Mattsson, N. Sandberg, and G. Grimvall, Phys. Rev. B **67**, 054101 (2003).
 - ²⁸ K. Nordlund and R.S. Averback, Phys. Rev. Lett. **80**, 4201 (1998).
 - ²⁹ D.A. Andersson, and S.I. Simak, Phys. Rev. B **70**, 115108 (2004).
 - ³⁰ J.P. Perdew, Y. Wang and E. Engel, Phys. Rev. Lett. **66**, 508 (1991)
 - ³¹ K. Carling, G. Wahnström, T. R. Mattsson, A. E. Mattsson, N. Sandberg, and G. Grimvall, Phys. Rev. Lett. **85**, 3862 (2000)
 - ³² C.L. Kelchner, S.J. Plimpton and J.C. Hamilton, Phys. Rev. B **58**, 11085 (1998).
 - ³³ V. Gavini, Phys. Rev. Lett. **101**, 205503 (2008).
 - ³⁴ P. Vinet, J. H. Rose, J. Ferrante and J. R. Smith, J. Phys.:Condens. Matter **1**, 1941 (1989).
 - ³⁵ G. Grimvall, *Thermophysical Properties of Materials* (Elsevier, Amsterdam, 1999).